Accepted Manuscript

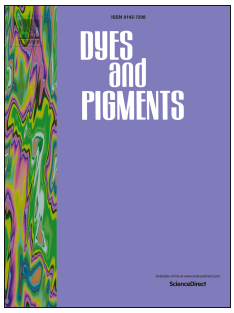

Rational design of slightly twisted coumarin molecules with remarkable solution and solid dual efficient luminescence

Yue Sun, Tong Wu, Fang Zhang, Rong Zhang, Min Wu, Yuezhen Wu, Xiaozhong Liang, Kunpeng Guo, Jie Li

PII: S0143-7208(17)31625-X

DOI: 10.1016/j.dyepig.2017.09.060

Reference: DYPI 6286

To appear in: *Dyes and Pigments*

Received Date: 28 July 2017

Revised Date: 18 September 2017

Accepted Date: 25 September 2017

Please cite this article as: Sun Y, Wu T, Zhang F, Zhang R, Wu M, Wu Y, Liang X, Guo K, Li J, Rational design of slightly twisted coumarin molecules with remarkable solution and solid dual efficient luminescence, *Dyes and Pigments* (2017), doi: 10.1016/j.dyepig.2017.09.060.

Graphical Abstract

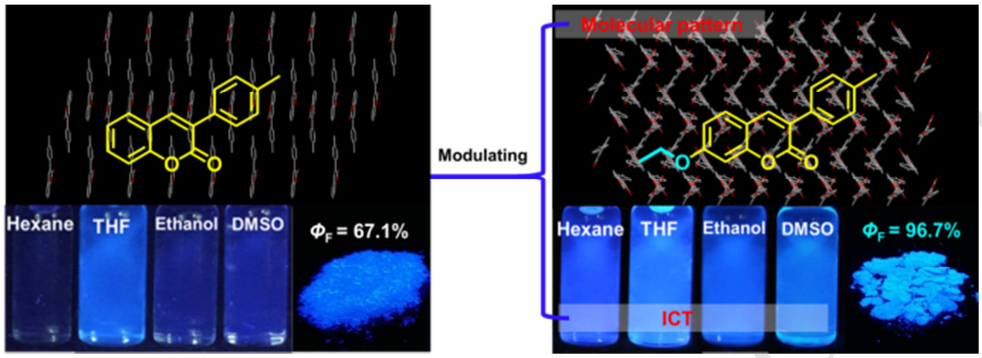

Dual efficient slightly twisted coumarin derivatives in solution and solid were realized by modulating intramoleculat charge transfer (ICT) and molecular pattern in crystal.

Rational design of slightly twisted coumarin molecules with remarkable solution and solid dual efficient luminescence

Yue Sun,[b] Tong Wu,[a, b] Fang Zhang,[a] Rong Zhang,[a] Min Wu,[a] Yuezhen Wu,[a] Xiaozhong Liang,[a] Kunpeng Guo,[a*] Jie Li[a*]

a Ministry of Education Key Laboratory of Interface Science and Engineering in Advanced Materials, Research Center of Advanced Materials Science and Technology, Taiyuan University of Technology, Taiyuan, 030024, China.

b School of Chemistry and Chemical Engineering, Taiyuan University of Technology, Taiyuan 030024, China.

Corresponding Author: guokunpeng@tyut.edu.cn; lijie01@tyut.edu.cn

Abstract

Endowing slightly twisted molecules highly emissive in both solution and solid state is of great importance for understanding the principle of maximizing the luminescent efficiency of luminophores. To this end, a series of slightly twisted coumarin luminophores **CM**s with different alkoxyl substituents at the 7-positions were synthesized. The effect of the substitutes on the diversity photophysical properties of the four compounds in solution, THF/H_2O mixtures and solid state were investigated. Comparing to the referenced compound **CM** (3-*p*-tolyl-2H-chromen-2-one) that without a substitute, the introduced electron-rich alkoxyl substitutes not only enhanced the intramolecular charge transfer (ICT) effect, but also significantly modified their molecular packing patterns in the crystals. The combined effect of increasing the radiative and suppressing the nonradiactive pathways boosted the luminescence efficiency of **CM1-CM3** in solution and the solid state simultaneously. Eventually, compound **CM2** with an ethoxyl substitute exhibited the strongest blue

emission with fluorescence quantum yields as high as 73.2% and 96.7% in solution and the solid state, respectively. This work presents an efficient strategy towards dual strong fluorescent luminophores in both solution and the solid state.

KEYWORDS: coumarin derivatives; slightly twisted conformation; intramolecular charge transfer; molecular packing pattern; dual efficient luminescence

1. Introduction

Highly emissive organic materials have attracted great attention due to their applicability in the fields of optoelectronic devices, chemosensors and bioprobes [1-18]. Although the emission of a number of traditional organic luminophores is efficient in dilute solution, it tends to decrease or even quench in the aggregated or solid states [19-22]. This aggregation-caused quenching (ACQ), which mainly caused by internal conversion, intersystem crossing, intermolecular electron transfer, as well as excimer or exciplex formation and isomerization, significantly limits the organic luminophores for their practical applications [23]. To prevent or alleviate these nonradiative pathways, numerous endeavors through molecular engineering and physical technology have been made, including the introduction of bulky substituents, enhanced intramolecular charge transfer (ICT) transition, cross-dipole packing and aggregated formation [24-34]. In 2001, Tang's group reported a series of silole derivatives with propeller-like conformations that was nonemissive in dilute solitions, but highly luminescent when aggregated into solid state [35]. Their work has attracted huge attention as an effective methodology to overcome ACQ, and this novel

phenomenon was termed as aggregation-induced emission (AIE). Since then, various AIE materials with efficient luminescence in the solid state have been prepared for diverse applications [36-40].

To realize intense luminescence in the solid state, most AIE molecules adopt highly twisted conformations to restrict intramolecular rotation (RIR) or adverse intermolecular interactions [41-47]. However, such molecules often emit weak emission in solution, which limits their wide range of applications. Studies of developing molecules possess intense luminescence in both solution and the solid state have, to the best of our knowledge, been focused on restricting free rotation of a single bond in twisted AIE molecules through conjugation-induced rigidity or increasing steric hindrance [48-50]. However, the exploration of dual efficient luminescent materials based on slightly twisted molecules is still challenging. This is probably arisen from the difficulties of luminescence optimization from molecular level to molecular packing pattern control in solution and the solid state.

Coumarin (chromen-2-one) derivatives have been widely studied and become a class of fluorescent dyes of intense interest due to their promising applications in organic lasers, organic light-emitting diodes and fluorescent sensors [51-59]. It is well known coumarin derivatives give intense emission in solution, but poor luminescence in the aggregated and solid state because their planar skeletons are prone to form strong π-π stacking [60]. To expand their real-world utilization, an AIE coumarin derivative based on the RIR mechanism has been designed and synthesized [61]. However, the reported AIE coumarin derivative still emits weakly in its solution. Thus,

the exploration of facile ways to obtain dual efficient fluorescent coumarin derivatives, especially those with slightly twisted conformations, is of high importance for structure-property understanding and practical applications. Herein, we developed four coumarin derivatives (Scheme 1) and investigated their photophysical properties systematically. Comparing with the referenced compound **CM** **(**3-*p*-tolyl-2H-chromen-2-one), its alkoxyl substituted derivatives at the 7-positions **CM1**-**CM3** showed boosted luminescence in both solution and the solid state due to the synergistic effect of the ICT characteristic and the molecular packing modification by the alkoxyl tail. Among them, **CM2** with an ethoxyl substitute exhibited the strongest blue emission with absolute fluorescence quantum yields (Φ_Fs) of 73.2% and 96.7% in THF solution and the solid state, respectively.

2. Experimental section

2.1. Materials and Characterization

All chemicals for synthesis were purchased from Energy Chemical and used without purification. Reactions were monitored by TLC silica plate (60F-254). NMR spectra measurements were carried out at Bruker 600 MHz for ^{1}H NMR and 151 MHz for ^{13}C NMR, using chloroform-d as the solvent. Chemical shifts were reported in parts per million (ppm) relative to internal TMS (0 ppm). Splitting patterns were described as singlet (s), doublet (d), triplet (t), quartet (q), or multiplet (m). Mass spectra were measured on Microflex MALDI-TOF mass spectrometer. UV-Vis spectra were recorded in a HITIACH U-3900 spectrometer. Photoluminescent (PL) spectra were

recorded in a HORIBA FluoroMax-4 spectrometer. The absolute fluorescence quantum yields (Φ_F) of solutions (10 μM) and powders were measured on HORIBA FluoroMax-4 by using a calibrated integrating sphere. The quartz cuvettes used were of 1 cm path length. Powder X-ray diffraction (XRD) of the samples was characterized using a Philips high resolution X-ray diffraction system (model PW1825). X-ray single-crystal diffractions of **CM** and **CM2** were performed on a Bruker SMART APEX II diffractometer with Mo Ka radiation (λ= 0.71000 Å). The structures were solved with direct method (SHELX-97) and refined with full-matrix least-squares technique. All non-hydrogen atoms were refined anistropically and hydrogen atoms were geometrically placed. Relevant crystal collection data, refinement data for the crystal structures and the cif files of **CM** and **CM2** can be found in the supporting information (ESI). The transient photoluminescence decay profiles of the solids were recorded using an Edinburgh Instrument FLS980 spectrometer equipped with an EPL-375 picosecond pulsed diode laser.

2.2. Synthetic procedures

*2.2.1. 3-p-Tolyl-2H-chromen-2-one (**CM**)*

An acetic anhydride (15 mL) solution of compound 2-hydroxybenzaldehyde (2.0 g, 16.4 mmol), 2-*p*-tolylacetic acid (2.46 g, 16.4 mmol) and several drops of triethylamine (5 mL) were charged sequentially into a three-necked flask. The mixture was heated to reflux till no raw material was detected by the TLC plate. After cooling the reaction mixture, the precipitation was filtered and recrystallized from ethanol to produce **CM** as white crystals (2.83 g, yield 72%). ^{1}H NMR (600 MHz, $CDCl_3$) δ =

7.79 (s, 1H), 7.61 (d, *J* = 8.1 Hz, 2H), 7.54 – 7.49 (m, 2H), 7.36 (d, *J* = 8.2 Hz, 1H), 7.30 – 7.26 (m, 2H), 7.25 (s, 1H), 2.40 (s, 3H). ^{13}C NMR (151 MHz, CDCl3) δ = 163.59, 156.34, 142.10, 141.82, 134.73, 134.09, 132.09, 131.32, 131.21, 130.73, 127.35, 122.69, 119.32, 24.21. MALDI-TOF: m/z $[M]^+$ cacld. $C_{16}H_{12}O_2$, 236.2653; found: 236.2651. Anal. Calcd for $C_{16}H_{12}O_2$: C, 81.34; H, 5.12; O, 13.54. Found: C, 81.29; H, 5.15; O, 13.56.

*2.2.2. 7-Hydroxy-3-p-tolyl-2H-chromen-2-one (**CM-OH**)*

An acetic anhydride (20 mL) solution of compound 2,4-dihydroxybenzaldehyde (4.0 g, 29 mmol), 2-*p*-tolylacetic acid (4.4 g, 29 mmol) and several drops of triethylamine (5 mL) were charged sequentially into a three-necked flask. The mixture was heated to reflux till no raw material was detected by the TLC plate. After cooling the reaction mixture, the precipitation was filtered and recrystallized from ethanol to produce **CM-OH** as a yellow solid (5.3g, yield 72%). ^{1}H NMR (600 MHz, CDCl3) δ = 7.78 (s, 1H), 7.60 (d, *J* = 8.1 Hz, 2H), 7.54 (d, *J* = 8.4 Hz, 1H), 7.27 (s, 1H), 7.26 (s, 1H), 7.15 (d, *J* = 2.1 Hz, 1H), 7.07 (dd, *J* = 8.4, 2.2 Hz, 1H), 2.40 (s, 3H). ^{13}C NMR (151 MHz, CDCl3) δ = 171.67, 163.22, 156.82, 155.57, 141.90, 141.47, 134.53, 132.11, 131.40, 131.27, 130.58, 121.34, 120.51, 112.84, 24.20, 24.04. MALDI-TOF: m/z $[M]^+$ cacld. $C_{16}H_{12}O_3$, 252.2647; found: 252.2644. Anal. Calcd for $C_{16}H_{12}$O3: C, 76.18; H, 4.79; O, 19.03. Found: C, 76.21; H, 4.74; O, 19.05.

*2.2.3. 7-Methoxy-3-p-tolyl-2H-chromen-2-one (**CM1**)*

A CH_3CN (50 mL) solution of compound **CM-OH** (2.0 g, 7.9 mmol), methyl iodide (1.3 g, 9.5 mmol) and K_2CO_3 (1.5 g, 10.9 mmol) was stirred at 80 ^oC for 12 hours till no raw material was detected by the TLC plate. After cooling to room temperature, mixture was poured into water and the precipitated yellow solid was filtered. The crude product was purified by silica gel column chromatography with petroleum: ethylacetate (15: 1,v: v) as eluent to afford **CM1** as a white powder (1.5 g, yield 71%). ^1H NMR (600 MHz, $CDCl_3$) δ= 7.73 (s, 1H), 7.60 – 7.58 (m, 2H), 7.42 (t, J = 5.2 Hz, 1H), 7.26 – 7.23 (m, 2H), 6.88 – 6.85 (m, 2H), 3.89 (s, 3H), 2.39 (s, 3H). ^{13}C NMR (151 MHz, $CDCl_3$) δ = 165.39, 163.80, 158.13, 142.20, 141.29, 135.05, 132.01, 131.64, 131.16, 127.71, 116.36, 115.56, 103.34, 58.66, 32.60, 24.13. MALDI-TOF: m/z $[M]^+$ cacld. $C_{17}H_{14}O_3$, 266.2913; found: 266.2915. Anal. Calcd for $C_{17}H_{14}O3$: C, 76.68; H, 5.30; O, 18.02. Found: C, 76.61; H, 5.26; O, 18.13.

*2.2.4. 7-Ethoxy-3-p-tolyl-2H-chromen-2-one (**CM2**)*

A procedure similar to the synthesis of **CM1** was followed but using bromoethane (1.0 g, 9.5 mmol) instead of methyl iodide. **CM2** was obtained as a white powder (1.7 g, yield 79%). 1H NMR (600 MHz, CDCl3) δ 7.73 (s, 1H), 7.59 (d, J = 8.1 Hz, 2H), 7.41 (d, J = 8.4 Hz, 1H), 7.25 (d, J = 8.0 Hz, 2H), 6.85 (dt, J = 4.0, 2.2 Hz, 2H), 4.11 (q, J = 7.0 Hz, 2H), 2.39 (s, 3H), 1.47 (t, J = 7.0 Hz, 3H). 13C NMR (151 MHz, CDCl3) δ = 164.76, 163.93, 158.11, 142.33, 141.28, 135.07, 132.02, 131.62, 131.16, 127.54, 116.21, 115.97，103.77, 67.07, 32.61, 24.16, 17.49. MALDI-TOF: m/z $[M]^+$

cacld. $C_{18}H_{16}O_3$, 280.3718; found: 280.3715. Anal. Calcd for $C_{18}H_{16}O3$: C, 77.12; H, 5.75; O, 17.12. Found: C, 77.08; H, 5.77; O, 17.15.

*2.2.5. 7-Butoxy-3-p-tolyl-2H-chromen-2-one (**CM3**)*

A procedure similar to the synthesis of **CM1** was followed but using 1-bromobutane (1.3 g, 9.5 mmol) instead of methyl iodide. **CM3** was obtained as a white powder (2.5 g, yield 85%). ^{1}H NMR (600 MHz, $CDCl_3$) δ = 7.73 (s, 1H), 7.60 – 7.58 (m, 2H), 7.41 (d, *J* = 8.4 Hz, 1H), 7.25 – 7.23 (m, 2H), 6.85 (dt, *J* = 3.3, 2.3 Hz, 2H), 4.03 (t, *J* = 6.5 Hz, 2H), 2.39 (s, 3H), 1.81 (dd, *J* = 14.8, 7.0 Hz, 2H), 1.51 (dd, *J* = 10.3, 4.7 Hz, 2H), 1.00 (t, *J* = 7.4 Hz, 3H). ^{13}C NMR (151 MHz, $CDCl_3$) δ = 164.97, 163.94, 158.12, 142.34, 141.26, 135.09, 132.02, 131.60, 131.16, 127.49, 116.17, 116.00, 103.78, 71.26, 33.94, 32.62, 24.17, 22.10, 16.72. MALDI-TOF: m/z $[M]^+$ cacld. $C_{20}H_{20}O_3$, 308.3710; found: 308.3708. Anal. Calcd for $C_{20}H_{20}O3$: C, 77.90; H, 6.54; O, 15.57. Found: C, 77.86; H, 6.51; O, 15.63.

3. Results and discussion

3.1 Synthesisand characterization

The target coumarin homologues **CM** and **CM1-CM3** were synthesized according to literatures as depicted in Scheme 2 [62]. Compounds **CM1-CM3** were synthesized by the alkoxylation reaction of the key intermediate **CM-OH** with methyl iodide, bromoethane and 1-bromobutane, respectively. They were all characterized by ^{1}H NMR, ^{13}C NMR, and mass spectroscopy. All of the coumarin derivatives are soluble

in common organic solvents such as toluene, tetrahydrofuran (THF), ethanol and dimethyl sulfoxide (DMSO).

3.2 Theoretical calculations

To understand the conformations of these compounds, the optimized molecular geometries were first evaluated by DFT calculation at the B3LYP/6-31G* level (Fig.1). The dihedral angles between the chromen-2-one and the 4-methylphenyl moiety for **CM**, **CM1**, **CM2** and **CM3** were 36.22°, 36.39°, 34.64° and 35.96°, respectively, indicating all of the compounds adopted slightly twisted conformations. Meanwhile, the four compounds presented similar frontier orbital distributions. As shown in Fig. S1, large steric overlap between the highest occupied molecular orbital (HOMO) and the lowest unoccupied molecular orbital (LUMO) was observed, which were mainly distributed over the conjugated chromen-2-one and the 4-methylphenyl segment. Although the alkoxyl substitutes in **CM1-CM3** hardly made contributions to the distribution of the molecular orbits, they did have a significant effect on the dipole moment of the molecules. Comparing to the referenced **CM** (4.0758 D), it was found increased dipole moments for **CM1** (5.7458D), **CM2** (5.9456D) and **CM3** (5.7857D), respectively, indicating an improved ICT effect of **CM1**, **CM2** and **CM3.**

3.3 Photophysical properties in solution

To verify the increased ICT effect on the photophysical properties of the compounds, UV-vis absorption and photoluminescence spectra were studied in solvents with different polarities and the corresponding data were extracted in Table 1. A bathochromic shift of the absorption bands from 328-330 nm for **CM** to 338-346 nm

for **CM1-CM3** was observed (Fig.2), which can be attributed to the introduced electron-rich alkoxyl substitutes at the 7-position in coumarin skeleton [63]. Meanwhile, **CM** showed similar absorption maxima and profiles in solutions, indicating a small change of dipole moment at the ground state in different solvents [64]. However, the absorption maxima (λ_{Abs}) of **CM1-CM3** red-shifted about 15 nm on increasing the solvent polarity from hexane to DMSO. These features indicate that ICT character has more evident influence on the absorption bands of **CM1-CM3** than that of **CM**.

The ICT effect introduced by the alkoxyl substitutes in coumarin skeleton was further confirmed in the photoluminescence spectra (Fig. 3). All of the four compounds gave blue emission in various solutions (Fig.4). The maximum emission peak (λ_{PL}) of **CM** was blue shifted from 425 nm to 409 nm as increasing the solvent polarity from nonpolar hexane to polar DMSO. This negative fluorosolvatochromism indicated that the molecule became less polar in the excited state than in the ground state [65]. On the contrary, the emission spectra of **CM1-CM3** showed positive fluorosolvatochromism with unstructured peaks shifted to the long wavelength as increasing the solvent polarity owning to the ICT effect of the molecules (Fig. 3b-3d, Table 1).

To further evaluate the influence of alkoxyl substitutes on the photoluminescent properties of **CM** and **CM1-CM3**, their Φ_Fs were examined. The Φ_Fs of the compounds increased with solvent polarity just in the primary region, and decreased in the very strong polar solvents, producing a distinct maximum. This up-down

phenomenon has been observed in some enone derivatives [66]. From hexane to THF, the increased Φ_F of "negative solvation effect" can be ascribed to the reduction of "the proximity effect" of π-π* and n-π* transition of the molecule with the increased solvent polarity [67]. With a further increase of the solvent polarity from THF to DMSO, the decreased Φ_F of "positive solvation effect" is attributed to the domination of the ICT process. In addition, the Stokes shifts of **CM** in various solvents were larger than those of **CM1-CM3**. This suggests a larger excitation-induced geometry change exists in **CM** than those in **CM1-CM3** in solution, and such "conformation change" decreases the Φ_F of **CM** [68]. All of the competing mechanisms resulted in the observed maximum fluorescence quantum yields of 17.6%, 45.8%, 73.2% and 61.06% for **CM**, **CM1**, **CM2** and **CM3** in THF, respectively. Obviously, **CM1-CM3** with enhanced ICT effect exhibited more efficient luminescence in solution than the referenced compound **CM** (Fig.4). Among them, **CM2** with an ethoxyl substitute exhibited the strongest blue emission, whose Φ_F value was about 4.1 times larger than that of **CM** in THF solution. Considering their similar slightly twisted skeletons, the reasonable explanation for the ethoxyl effect is that **CM2** possesses the largest dipole moment among the four compounds, leading to more obvious ICT effect to give highly efficient luminescence in solution.

3.4 Fluorescent properties in the aggregated states

To investigate the fluorescence behaviors of **CM** and **CM1-CM3** in aggregated states, the UV-Vis absorption and PL spectra in THF/water mixtures with different water fractions (f_w) were studied. When the f_w was up to 90%, the absorption spectra

exhibited significant changes with leveled-off tails clearly appearing in the long-wavelength region (Fig. S2). This result can be attributed to the well-known Mie effect, which indicates that **CM** and **CM1**-**CM3** molecules aggregate in high water fractions. In the PL spectra, all of the compounds exhibited an up-down tendency in intensity upon increasing the water fraction. Taking **CM2** as a typical example, its PL intensity was increased upon increasing water content when the water fraction was less than 80%, but sharply decreased with emission peak shifting 17 nm to long wavelength when the f_w reached 99%, indicating *J*-type nanoaggregates may be formed during aggregation (Fig. 5). Similar behaviors were observed for compounds **CM**, **CM1** and **CM3** (Fig.S3), respectively. This up-down phenomenon has been observed in some compounds with AIE properties, suggesting the aggregates morphology of the coumarin derivatives at high water content is different from that at lower water content [69]. SEM images in Fig. 6 and Fig. S4 gave a visualized proof to support our hypothesis. **CM2** formed amorphous nanoscale aggregates in mixtures with "low" water content (f_w < 80%) (Fig. 6a), and further developed to nanoparticles which gave intense emission when f_w reached 80% (Fig. 6b). Further increasing the f_w to 99%, regular 1D rods were observed (Fig. 6c), which may cause emission quench because of the dominated *J*-aggregates.

3.5 Fluorescent properties in the solid states

Although **CM** and **CM1-CM3** aggregates exhibited similar photophysical properties in THF/water mixtures, their crystals gave distinct fluorescence behaviors. As shown in Fig. 7a and Table 2, **CM** crystals emitted blue fluorescence peaking at

441 nm with a moderate Φ_F of 67.1% under UV irradiation. However, the crystals of **CM1**, **CM2** and **CM3** gave red-shifted emission of 450 nm, with a dramatically enhanced Φ_F value of 89.6%, 96.7% and 70.7%, respectively. Similar to the fluorescence behavior in solutions, the crystal of **CM2** showed the strongest blue emission, whose Φ_F value was about 1.44 times larger than that of **CM**. Time-resolved fluorescence measurements revealed a longest lifetime of **CM2** crystals (4.39 ns) than any other crystals of the compounds (Fig. 7b and Table 2). The highest Φ_F value, combined with a longest lifetime, led to a relatively large radiative decay rate (k_r 0.22 ns^{-1}) and a smallest nonradiative decay rate (k_{nr} 0.0075 ns^{-1}) of **CM2** crystals, which suggested the absolute domination of radiative decay.

To explore the underlying origins of the enhanced emission of alkoxyl substituted coumarins, the molecular packing patterns in single crystals were analyzed through X-ray diffraction experiments and the crystallographic data were summarized in Table S1. As shown in Fig. 8, both **CM** (CCDC1561738) and **CM2** (CCDC 1561739) molecules adopted slightly twisted conformations, and the dihedral angles of between the chromen-2-one and the 4-methylphenyl moiety at the 3- position were 28.7°, and 37.53°, respectively, which was close to their calculated results. Notably, their molecular packing patterns were significantly different from each other. **CM** crystallized in monoclinic $P2_1/c$ symmetry (Fig. 9a and 9b). In the crystal, the molecules were stacked in an anti-parallel arrangement to form a lamellar-packed mode viewed down the *b*-axis. The interplanar distance (3.393 Å) between the adjacent chromen-2-one moieties demonstrated efficient π-π stacking in crystal that

would activate nonradiative pathways of excited states causing fluorescence quenching. On the other hand, multiple O...H hydrogen bonds with distances about 2.56 Å were observed between the aromatic H and the carbonyl groups of adjacent molecules. These hydrogen bonds can rigidify the molecular conformation of **CM** in the solid thus suppress the nonradiative pathways and resulted emission intensity increasing. As a result, **CM** crystals demonstrated a moderate Φ_F because of the competitive intermolecular interactions of π-π stacking and hydrogen bonds. However, in the case of **CM2**, dramatic changes took place after the introduction of an ethoxyl substitute at the 7-position of **CM** in the stacking pattern and intermolecular interactions (Fig. 9c and 9d): 1) **CM2** crystallized in triclinic P-1 symmetry. The molecules formed herringbone packing in a face-to-edge pattern without π-π overlap between two adjacent molecules; 2) two main kinds of intermolecular weak interactions were observed including multiple O…H hydrogen bonds with distances in the range of 2.56-2.71 Å, and C-H…π interactions with distances about 2.8 Å between the aromatic H and the chromen-2-one moiety as well as the alkoxyl H and the aromatic ring of adjacent molecules. Therefore, the nonradiative pathways were effectively weakened or eliminated due to the beneficial hydrogen bonds and C-H…π interactions as well as the absence of the adverse π-πinteractions, raising the emission intensity of **CM2** crystal to give a Φ_F as high as 96.7%.

4. Conclusion

In summary, we developed a molecular design strategy for boosting the luminescence efficiency both in solution and the solid state of coumarin derivatives

with slightly twisted conformation. By attaching electron-rich alkoxyl tails at the 7-position of **CM** the fluorescent efficiencies of **CM1**-**CM3** in solution were enhanced up to 73.2% through the introduced ICT effect. Meanwhile, the alkoxyl tail plays a key role in modulating the molecular packing patterns and controlling the intermolecular interactions to enhance the solid efficiency of **CM1**-**CM3**. Both the face-to-edge packing patterns that eliminated π-π intermolecular interactions and beneficial weak intermolecular interactions suppressed nonradiative pathways in crystal, endowing **CM2** with remarkable solid efficiency of 96.7%. Such strategy of simultaneously taking advantages of ICT effect and modulating molecular packing patterns provides an effective method to construct dual-state highly luminescent materials in both solution and the solid state, which would expand their practical applications in optoelectronic and biological fields.

Acknowledgements

We thank the National Natural Science Foundation of China (61605138), the Qualified Personnel Foundation of Taiyuan University of Technology (QPFT) (No: tyutrc-201255a), Shanxi Province Science Foundation for Youths (201701D221038), and the Shanxi Provincial Key Innovative Research Team in Science and Technology (201513002-10).

References

[1] Shimizu M, Takeda Y, Higashi M, Hiyama T. 1,4-Bis(alkenyl)-2,5-dipiperidinobenzenes: minimal fluorophores exhibiting highly efficient emission in the solid state. Angew Chem Inter Ed 2009;48:3653–

6.

[2] Chan CYK, Zhao ZJ, Lam JWY, Liu JZ, Chen SM, Lu P, et al. Efficient light emitters in the solid state: synthesis, aggregation-induced emission, electroluminescence, and sensory properties of luminogens with benzene cores and multiple triarylvinyl peripherals. Adv Funct Mater 2012;22:378–89.

[3] Sun HB, Liu SJ, Lin WP, Zhang YK, Lv W, Huang X, et al. Smart responsive phosphorescent materials for data recording and security protection. Nat Commun 2014;5:3601.

[4] Luo JJ, Gong SL, Gu Y, Chen TH, Li YF, Zhong C, et al. Multi-carbazole encapsulation as a simple strategy for the construction of solution-processed, non-doped thermally activated delayed fluorescence emitters. J Mater Chem C 2016;4:2442–6.

[5] Ma Y, Liang H, Zeng Y, Yang HR, Ho C-L, Xu WJ, et al. Phosphorescent soft salt for ratiometric and lifetime imaging of intracellular pH variations. Chem Sci 2016;7:3338-46.

[6] Liu SJ, Zhou N, Chen ZJ, Wei HJ, Zhu YN, Guo S, et al. Using a redox-sensitive phosphorescent probe for optical evaluation of an intracellular redox environment. Opt Letter 2017;42:13-6.

[7] Shi HF, Ma X, Zhao Q, Liu B, Qu QY, An ZF, et al. Ultrasmall Phosphorescent Polymer Dots for Ratiometric Oxygen Sensing and Photodynamic Cancer Therapy. Adv Funct Mater 2014;24:4823-30.

[8] Yang ZG, Zhao N, Sun YM, Miao F, Liu Y, Liu X, et al. Highly selective red- and

green-emitting two-photon fluorescent probes for cysteine detection and their bio-imaging in living cells. Chem Commun 2012;48:3442-4.

[9] Shi HF, Sun HB, Yang HR, Liu SJ, Jenkins G, Feng W, et al. Cationic Polyfluorenes with Phosphorescent Iridium(III) Complexes for Time-Resolved Luminescent Biosensing and Fluorescence Lifetime Imaging. Adv Funct Mater 2013;23:3268-76.

[10] Chui C.-H., Wang Q, Chow W.-C., Yeun M.C.-W., Wong K.-L., Kwok W.-M., et al. 5-(Dimethylamino)-N-(4-ethynylphenyl)-1-naphthalenesulfonamide as a novel bifunctional antitumor agent and two-photon induced bio-imaging probe. Chem Commun 2010;46:3538-40.

[11] Liu SJ, Zhang YL, Liang H, Chen ZJ, Liu ZY, Zhao Q, Time-resolved luminescence imaging of intracellular oxygen levels based on long-lived phosphorescent iridium(III) complex. Opt Express 2016;24:15757-64.

[12] Liu SJ, Xu AA, Chen ZJ, Ma Y, Yang HR, Shi ZJ, et al. Phosphorescent ion-paired iridium(III) complex for ratiometric and time-resolved luminescence imaging of intracellular biothiols. Opt Express 2016;24:28247-55.

[13] Guo FQ, Tian MG, Miao F, Zhang WJ, Song GF, Liu Y, et al. Lighting up cysteine and homocysteine in sequence based on the kinetic difference of the cyclization/addition reaction. Org Biomol Chem 2013;11:7721-8.

[14] Tian MG, Guo FQ, Sun YM, Zhang WJ, Miao F, Liu Y, et al. A fluorescent probe for intracellular cysteine overcoming the interference by glutathione. Org Biomol Chem 2014;12:6128-33.

[15] Huang WB, Gu W, Huang HX, Wang JB, Shen WX, Lv YY, et al. A porphyrin-based fluorescent probe for optical detection of toxic Cd^{2+} ion in aqueous solution and living cells. Dyes Pigm 2017;143:427–35.

[16] Zhang RX, Li PF, Zhang WJ, Li N, Zhao N. A highly sensitive fluorescent sensor with aggregation-induced emission characteristics for the detection of iodide and mercury ions in aqueous solution. J Mater Chem C 2016;4:10479–85.

[17] Zhang GQ, Palmer GM, Dewhirst MW, Fraser CL. A dual-emissive-materials design concept enables tumour hypoxia imaging. Nat Mater 2009;8:747–51.

[18] Lan HC, Xue FF, Liu ZK, Chen L, Huang CH, Yi T. Evolution of rhodamine B into near-infrared dye by phototriggered radical reaction and its application for lysosome-specific live-cell imaging. Adv Opt Mater 2016;4:1367–72.

[19] Birks JB. Photophysics of Aromatic Molecules 1970.

[20] Anthony JE. Functionalized acenes and heteroacenes for organic electronics. Chem Rev 2006;106:5028–48.

[21] Figueira-Duarte TM, Müllen K. Pyrene-based materials for organic electronics. Chem Rev 2011;111:7260–314.

[22] Wen P, Gao ZX, Zhang R, Li A, Zhang F, Li J, et al. A–π–D–π–A carbazole derivatives with remarkable solvatochromism and mechanoresponsive luminescence turn-on. J Mater Chem C 2017;5:6136–43.

[23] Qin A, Tang BZ. Aggregation-induced emission: fundamentals and applications. Wliey, United Kingdom 2013.

[24] Zhu XH, Gindre D, Mercier N, Frère P, Nunzi JM. Stimulated emission from a

needle□like single crystal of an end□capped fluorine/phenylene Co□oligomer. Adv Mater 2003;15:906-9.

[25] Langhals H, Krotz O, Polborn K, Mayer P. A novel fluorescent dye with strong, anisotropic solid-state fluorescence, small stokes shift, and high photostability. Angew Chem Int Ed 2005;44:2427–8.

[26] Kaiser TE, Wang H, Stepanenko V, Würthner F. Supramolecular construction of fluorescent J-Aggregates based on hydrogen-bonded perylene dyes. Angew Chem Int Ed 2007;46:5541–4.

[27] Iida A, Yamaguchi S. Intense solid-state blue emission with a small stokes' shift: π-stacking protection of the diphenylanthracene skeleton. Chem Commun 2009:3002-4.

[28] Zhao CH, Wakamiya A, Inukai Y, Yamaguchi S. Highly emissive organic solids containing 2,5-Diboryl-1,4-phenylene unit. J Am Chem Soc 2006;128:15934–5.

[29] Wakamiya A, Mori K, Yamaguchi S. 3-boryl-2,2′-bithiophene as a versatile core skeleton for full-color highly emissive organic solids. Angew Chem Int Ed 2007;46:4273–6.

[30] Xie ZQ, Yang B, Li F, Cheng G, Liu LL, Yang GD, et al. Cross dipole stacking in the crystal of distyrylbenzene derivative: the approach toward high solid-state luminescence efficiency. J Am Chem Soc 2005;127:14152–3.

[31] Xue PC, Lu R, Chen GJ, Zhang Y, Nomoto H, Takafuji M, et al. Functional organogel based on a salicylideneaniline derivative with enhanced fluorescence emission and photochromism. Chemistry - Eur J 2007;13:8231–9.

[32] An BK, Kwon SK, Jung SD, Park SY. Enhanced emission and its switching in fluorescent organic nanoparticles. J Am Chem Soc 2002;124:14410–5.

[33] Kaiser TE, Wang H, Stepanenko V, Würthner F. Supramolecular construction of fluorescent J-aggregates based on hydrogen-bonded perylene dyes. Angew Chem Int Ed 2007;119:5637–40.

[34] Guo KP, Zhang F, Guo S, Li K, Lu XQ, Li J, et al. Achieving red/near-infrared mechanoresponsive luminescence turn-on: mechanically disturbed metastable nanostructures in organic solids. Chem Commun 2017;53:1309–12.

[35] Luo JD, Xie ZL, Lam JWY, Cheng L, Tang BZ, Chen H, et al. Aggregation-induced emission of 1-methyl-1,2,3,4,5-pentaphenylsilole. Chem Commun 2001;18:1740–1.

[36] Hong YN, Lam JWY, Tang BZ. Aggregation-induced emission: phenomenon, mechanism and applications. Chem Commun 2009;29:4332.

[37] Wang M, Zhang GX, Zhang DQ, Zhu DB, Tang BZ. Fluorescent bio/chemosensors based on silole and tetraphenylethene luminogens with aggregation-induced emission feature. J Mater Chem 2010;20:1858.

[38] Huang J, Jiang YB, Yang J, Tang RL, Xie N, Li QQ, et al. Construction of efficient blue AIE emitters with triphenylamine and TPE moieties for non-doped OLEDs. J Mater Chem C 2014;2:2028.

[39] Guo KP, Gao ZX, Cheng J, Shao Y, Lu XQ, Wang H. Linear thiophene-containing π-conjugated aldehydes with aggregation-induced emission for building solid red luminophors. Dyes Pigm 2015;115:166–71.

[40] Galer P, Korošec RC, Vidmar M, Šket B. Crystal structures and emission properties of the BF_2 complex 1-Phenyl-3-(3,5-dimethoxyphenyl)-propane-1,3-dione: multiple chromisms, aggregation- or crystallization-induced emission, and the self-assembly effect. J Am Chem Soc 2014;136:7383–94.

[41] Hong Y, Lam JWY, Tang BZ. Aggregation-induced emission. Chem Soc Rev 2011;40:5361.

[42] Yang ZY, Chi ZG, Yu T, Zhang XQ, Chen MN, Xu BJ, et al. Triphenylethylene carbazole derivatives as a new class of AIE materials with strong blue light emission and high glass transition temperature. Journal of Mater Chem 2009;19:5541.

[43] Ma Y, Zeng Y, Liang H, Ho, C-L, Zhao Q, Huang W, et al. A water-soluble tetraphenylethene based probe for luminescent carbon dioxide detection and its biological application. J Mater Chem C 2015;3:11850-6.

[44] Dong Y-J, Meng ZG, Ho C-L, Wong W-Y, A novel “turn-on” dipyrrin-type fluorescent detector of Zn^{2+} based on tetraphenylethene. Tetrahedron 2017;73:3305-9.

[45] Yang J, Guo QX, Wen XD, Gao XM, Peng Q, Li QQ, et al. Pyrene-based blue AIEgens: tunable intramolecular conjugation, good hole mobility and reversible mechanochromism. J Mater Chem C 2016;4:8506–13.

[46] Lu HG, Zheng YD, Zhao XW, Wang LJ, Ma SQ, Han XQ, et al. Highly efficient far red/near-infrared solid fluorophores: aggregation-induced emission,

intramolecular charge transfer, twisted molecular conformation, and bioimaging applications. Angew Chemie Inter Ed 2016;55:155–9.

[47] Han T, Zhang YJ, Feng X, Lin ZG, Tong B, Shi JB, et al. Reversible and hydrogen bonding-assisted piezochromic luminescence for solid-state tetraaryl-buta-1,3-diene. Chem Commun 2013;49:7049.

[48] Chen G, Li WB, Zhou TR, Peng Q, Zhai D, Li HX, et al. Conjugation-induced rigidity in twisting molecules: filling the gap between aggregation-caused quenching and aggregation-induced emission. Adv Mater 2015;27:4496–501.

[49] Li M, Niu YL, Zhu XZ, Peng Q, Lu HY, Xia AD, et al. Tetrahydro[5]helicene-based imide dyes with intense fluorescence in both solution and solid state. Chem Commun 2014;50:2993–5.

[50] Xue PC, Sun JB, Chen P, Gong P, Yao BQ, Zhang ZQ, et al. Strong solid emission and mechanofluorochromism of carbazole-based terephthalate derivatives adjusted by alkyl chains. J Mater Chem C 2015;3:4086–92.

[51] Duarte FJ, Hillman LW, Dye Laser Principles, with Applications. Academic Press Inc. : San Diego, CA, 1990.

[52] Liu XG, Cole JM, Waddell PG, Lin TC, Radia J, Zeidler A. Molecular origins of optoelectronic properties in coumarin dyes: toward designer solar cell and laser applications. J Phys Chem A 2012;116:727–37.

[53] Yang Y, Zou J, Rong H, Qian GD, Wang ZY, Wang MQ. Influence of various coumarin dyes on the laser performance of laser dyes co-doped into ORMOSILs. Appl Phys B 2007;86:309–13.

[54] Zhou X, Blochwitz-Nimoth J, Pfeiffer M, Maennig B, Drechsel J, Werner A, et al. Inverted transparent multi-layered vacuum deposited organic light-emitting diodes with electrically doped carrier transport layers and coumarin doped emissive layer. Synth Met 2003;138:193–6.

[55] Yu TZ, Zhang P, Zhao YL, Zhang H, Meng J, Fan DW. Synthesis, characterization and high-efficiency blue electroluminescence based on coumarin derivatives of 7-diethylamino-coumarin-3-carboxamide. Org Electron 2009;10:653–60.

[56] Borisov SM, Klimant I. Ultrabright oxygen optodes based on cyclometalated iridium(III) coumarin complexes. Anal Chem 2007;79:7501–9.

[57] Roussakis E, Pergantis SA, Katerinopoulos HE. Coumarin-based ratiometric fluorescent indicators with high specificity for lead ions. Chem Commun 2008;46:6221-3.

[58] Sarkar D, Ghosh P, Gharami S, Mondal TK, Murmu N. A novel coumarin based molecular switch for the sequential detection of Al^{3+} and F^{-}: application in lung cancer live cell imaging and construction of logic gate. Sens Actuators B Chem 2017;242:338–46.

[59] Samanta K, Rao CP. A bifunctional thioether linked coumarin appended calix[4]arene acquires selectivity toward Cu^{2+} sensing on going from solution to SAM on gold. ACS Appl Mater Interfaces 2016;8:3135–42.

[60] Kumar S, Singh P, Srivastava R, Koner RR, Pramanik A, Mathew J, et al. Engineering fused coumarin dyes: a molecular level understanding of aggregation

quenching and tuning electroluminescence via alkyl chain substitution. J Mater Chem C 2014;2:6637-47.

[61] Bu F, Duan RH, Xie YJ, Yi YP, Peng Q, Hu RR, et al. Unusual aggregation-induced emission of a coumarin derivative as a result of the restriction of an intramolecular twisting motion. Angew Chem Int Ed 2015;54:14492–7.

[62] Wu JS, Liu WM, Zhuang XQ, Wang F, Wang PF, Tao SL, et al. Fluorescence turn on of coumarin derivatives by metal cations: a new signaling mechanism based on C=N isomerization. Org Lett 2007;9:33–6.

[63] Jhun BH, Ohkubo K, Fukuzumi S, You Y. Synthetic control over intra- and intermolecular charge transfer can turn on the fluorescence emission of non-emissive coumarin. J Mater Chem C 2016;4:4556–67.

[64] Chen YJ, Ling Y, Ding L, Xiang CL, Zhou G. Quinoxaline-based cross-conjugated luminophores: charge transfer, piezofluorochromic, and sensing properties. J Mater Chem C 2016;4:8496–505.

[65] Babür B, Seferoğlu N, Seferoğlu Z. A ratiometric fluorescence chemosensor based on a coumarin–pyrazolone hybrid: the synthesis and an investigation of the photophysical, tautomeric and anion binding properties by spectroscopic techniques and DFT calculations. Tetra Lett 2015;56:2149–54.

[66] Wang P, Wu SK. A study on the spectroscopy and photophysics of 4’-N,N-dimethylaminoflavone derivatives. Journal Lumin 1994;62:33-9.

[67] Siebrand W, Zgierski MZ. Radiationless decay of vibronically coupled electronic

states. II. non□condon effects of nontotally symmetric accepting modes. J Chem Phys 1980;72:1641–6.

[68] Belletste M, Durocher G. Effects of small chemical variation, functionality, and solvent on the spectroscopic and photophysical properties of the 3H-indole probe fiuorophore. J Phys Chem 1992;96:9183-8.

[69] Cao YL, Yang MD, Wang Y, Zhou HP, Zheng J, Zhang XZ, et al. Aggregation-induced and crystallization-enhanced emissions with time-dependence of a new schiff-base family based on benzimidazole. J Mater Chem C 2014;2:3686–94.

Table1

Photophysical properties of **CM** and **CM1-CM3** in various solvents (10 μM).

Compound	Solvent	λ_{Abs} (nm)	λ_{PL} (nm)	Stokes shift (cm^{-1})	Φ_F (%)
CM	Hexane	328	425	6958	6.3
	THF	328	410	6098	17.6
	Ethanol	328	408	5978	4.7
	DMSO	330	409	5853	4.2
CM1	Hexane	338	414	6333	28.5
	THF	342	424	5655	45.8
	Ethanol	342	429	5930	41.2
	DMSO	345	431	5784	39.4
CM2	Hexane	338	416	5547	38.9
	THF	342	425	5710	73.2
	Ethanol	344	431	5868	71.5
	DMSO	345	433	5891	68.1
CM3	Hexane	338	416	5547	56.4
	THF	343	423	5514	61.1
	Ethanol	344	429	5760	59.7
	DMSO	346	431	5700	58.5

Table 2

Luminescent properties of **CM** and **CM1-CM3** in solid sates.

Compound	λ_{PL} (nm)	Φ_F (%)	τ (ns)	k_r(ns^{-1})	k_{nr}(ns^{-1})
CM	441	67.1	3.72	0.18	0.088
CM1	450	89.6	3.76	0.24	0.028
CM2	450	96.7	4.39	0.22	0.0075
CM3	450	70.7	3.79	0.19	0.077

Captions

Scheme 1 Molecular structures of **CM**, **CM1**, **CM2** and **CM**.

Fig. 1 Optimized molecular geometry of **CM**, **CM1**, **CM2** and **CM3** by DFT calculation at the B3LYP/6-31G* level.

Scheme 2 The synthetic route for compounds **CM**, **CM1**, **CM2** and **CM3**.

Fig. 2 Normalized absorption spectra of (a) **CM**, (b) **CM1**, (c) **CM2** and (d) **CM3** in various solvents (10 μM).

Fig. 3 Normalized PL spectra of (a) **CM**, (b) **CM1**, (c) **CM2** and (d) **CM3** in various solvents (10 μM).

Fig.4 Photographs of (a) **CM**, (b) **CM1**, (c) **CM2** and (d) **CM3** in various solvents under UV (λ_{ex}=365 nm) illumination.

Fig.5 (a) PL spectra of **CM2** (10 μM) in THF/water mixtures with different water fractions, (b) The effect of water fractions on the maximum emission intensity of **CM2**.

Fig. 6 SEM images of **CM2** aggregates in THF/water mixtures (10 μM) with different water fractions: (a) in THF/H_2O (60:40, v/v); (b) in THF/H_2O (20:80, v/v); (c) in THF/H_2O (1:99, v/v).

Fig.7 (a) PL emission spectra of **CM**, **CM1**, **CM2** and **CM3** in the solid state. Inset: photographs of **CM**, **CM1**, **CM2** and **CM3** powders under UV (λ_{ex}=365 nm) illumination. (b) Time-resolved fluorescence spectra of **CM**, **CM1**, **CM2** and **CM3** in the solid state (λex = 375 nm).

Fig.8 ORTEP diagram of (a) **CM** and (b) **CM2**.

Fig.9 (a) The packing pattern and (b) weak interactions in the crystals of **CM**. (c) The packing pattern and (d) weak interactions in the crystals of **CM2**.

Figures

Scheme 1

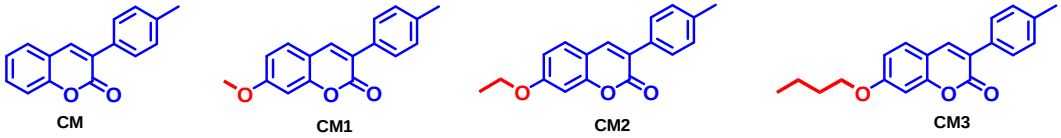

Figure 1

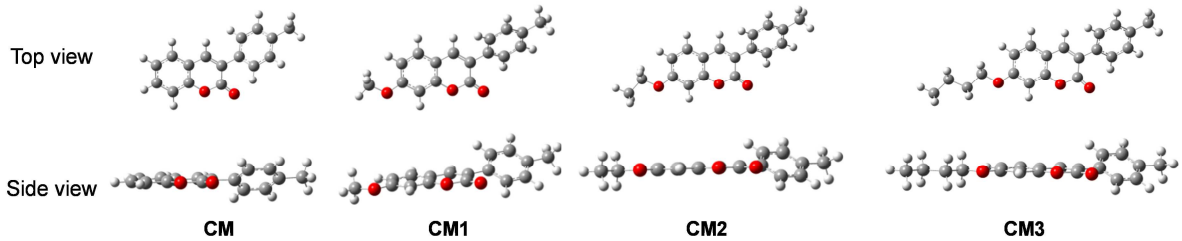

Scheme 2

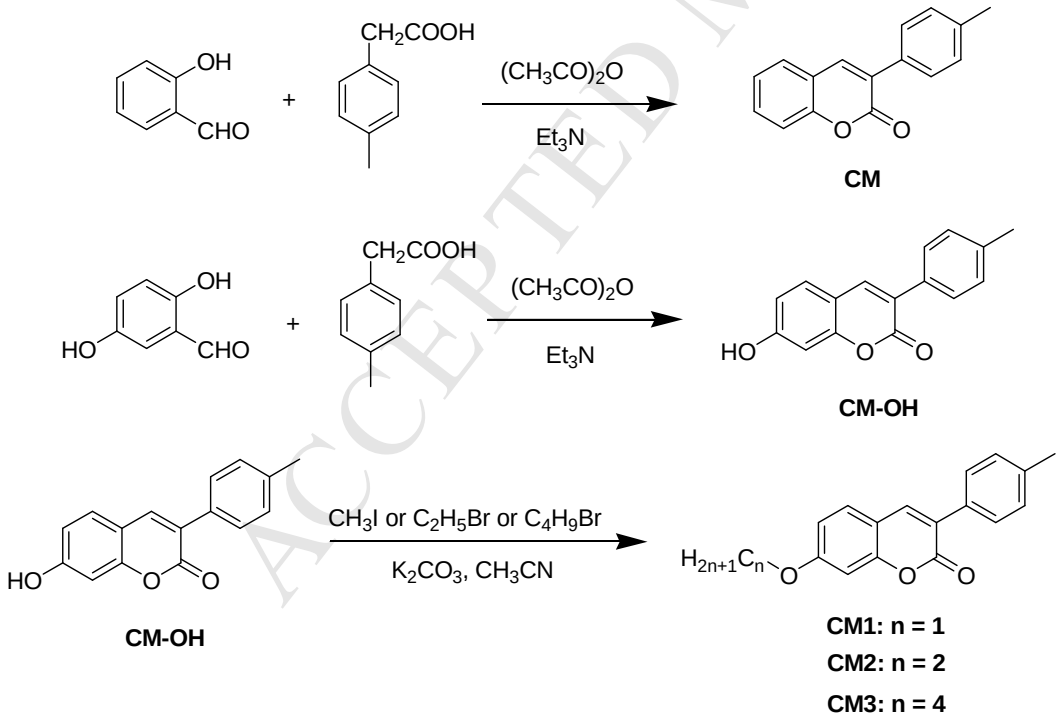

Figure 2

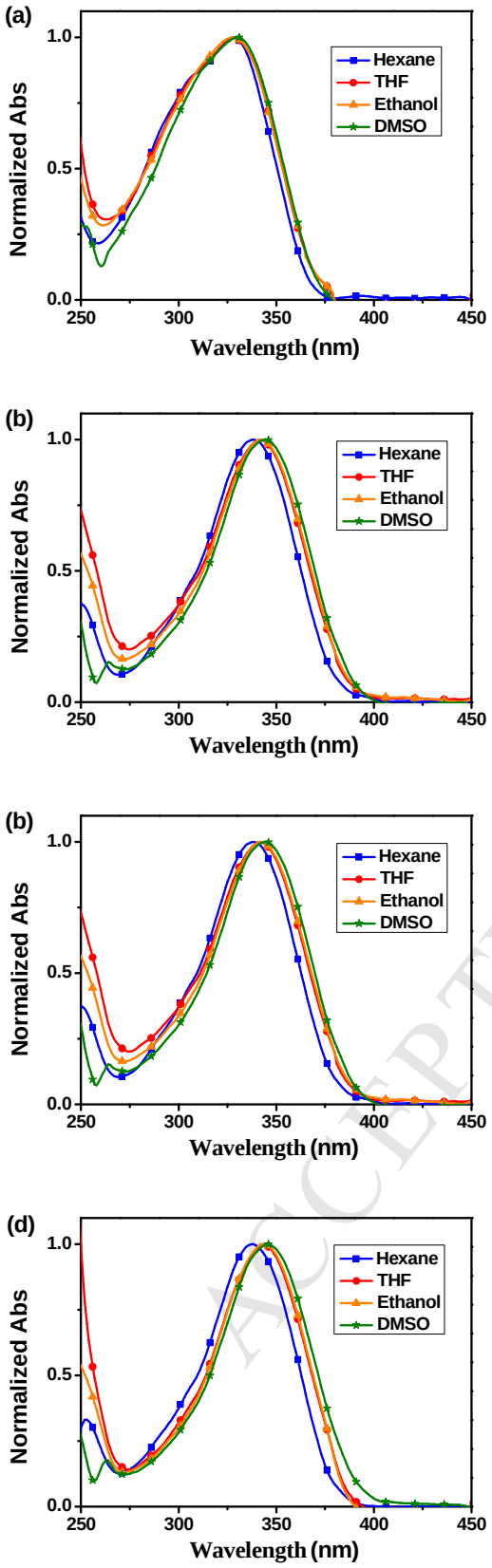

Figure 3

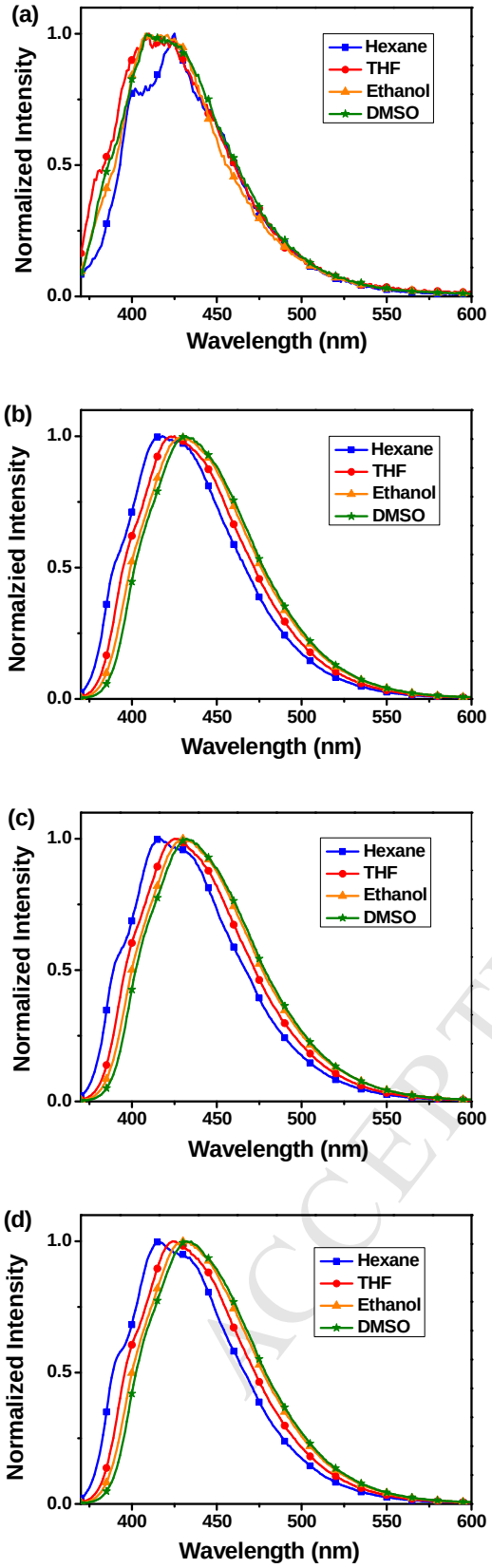

Figure 4

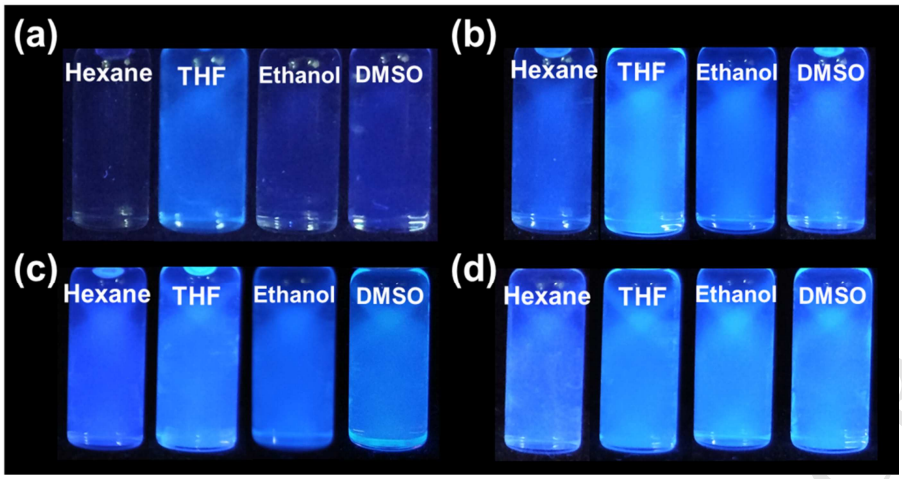

Figure 5

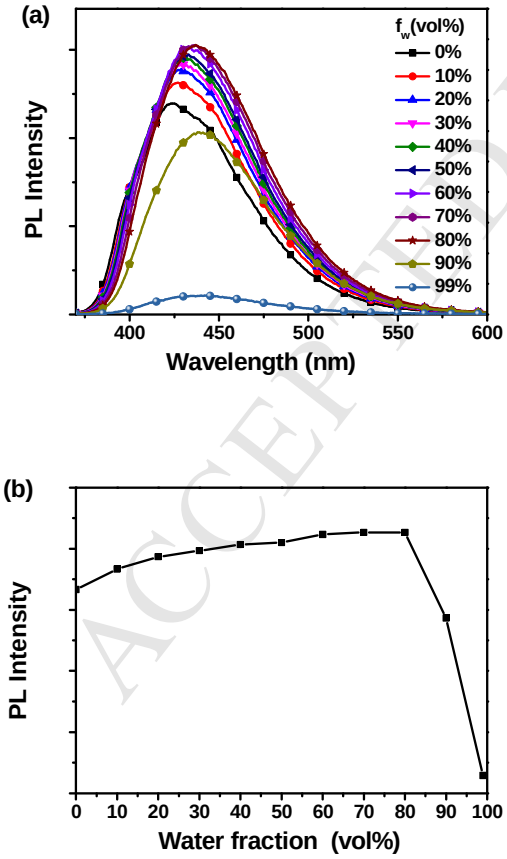

Figure 6

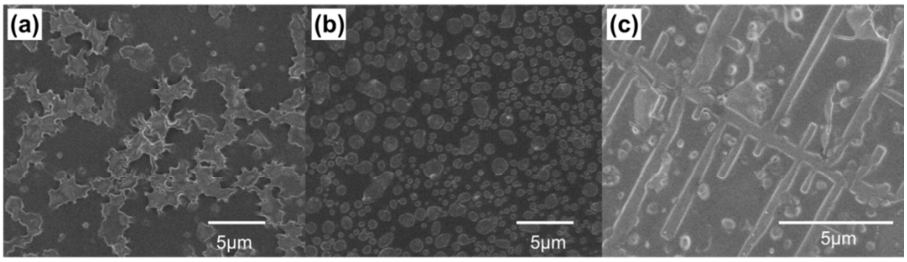

Figure 7

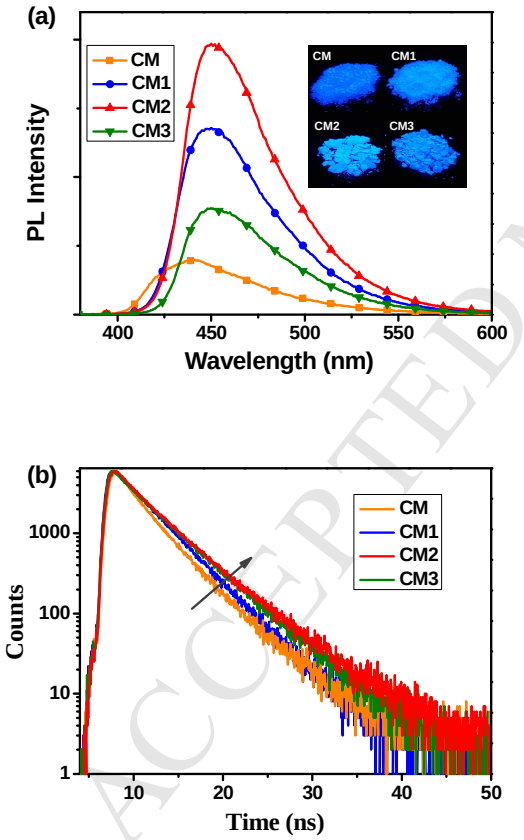

Figure 8

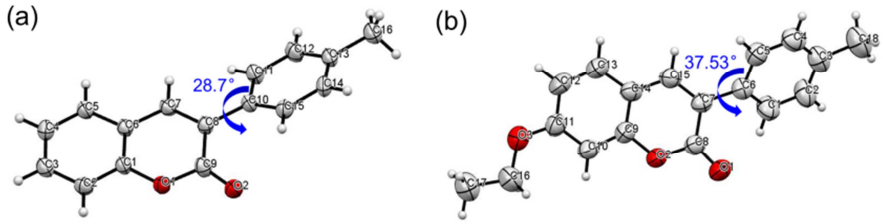

Figure 9

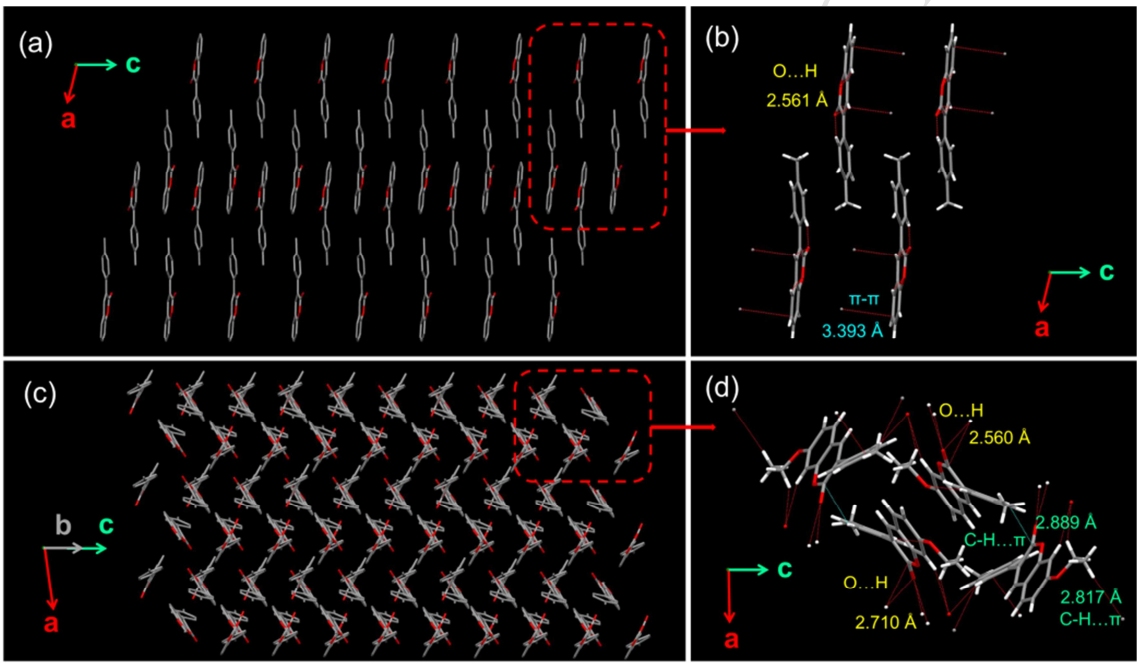

Highlights

- Four slightly twisted coumarin luminophores with different alkoxyl substituents at the 7-positions were synthesized.
- The introduced alkoxyl substitutes enhanced the intramolecular charge transfer effect and modified their molecular packing patterns in the crystals.
- Alkoxyl substituted **CM1-CM3** exhibited boosted luminescence in solution and the solid state simultaneously.
- **CM2** with an ethoxyl substitute giving fluorescence quantum yields as high as 73.2% and 96.7% in solution and the solid state, respectively.